Heat transport across hot - cold interface with magnetic field

Shule Li
Department of Physics and Astronomy, University of Rochester

December 2010

Abstract

The low temperature of the hot bubbles observed in the wind blown bubbles (WBB) remains a mystery for many years. It is assumed that the heat conduction plays an important role in the cooling of the hot bubbles. Meanwhile, in a stellar object such as WBB, the magnetic field can be strong and highly tangled which results in the anisotropic heat conduction which only allows the electrons to carry thermal energy along the magnetic field lines. A natural question is, in the situation such as a WBB, how would the heat transfer rate which relates to the hot bubble cooling rate be related with the magnetic field structure? In this study, we start from two simple cases: (1) field lines aligned with the hot bubble - cold shell interface; (2) field lines perpendicular to the hot bubble - cold shell interface. We explore the relation between the magnetic field topology and the heat transfer rate by adding tangled field to the above configuration and demonstrate that the degree of tanglement and the heat transfer rate has a simple mathematical relation which matches well with the analytical calculation. This relation can be useful in determining the heat transfer efficiency when there is a magnetic field in the environment of astrophysical context.

keywords: *magneto-hydrodynamics, planetary nebula, magnetic reconnection, wind blown bubbles, anisotropic heat conduction*

1 Introduction

The interface bounding hot and cold interstellar medium (ISM) exist in astrophysics problems of various scales. The thermal conduction through such interface is critical in determining the heating(cooling) process of the materials behind the interface. However, the thermal conduction in ISM is usually controlled by the magnetic field topology, which renders the electrons to move freely only along the field lines. This results in a strong thermal conductivity along the field lines and weak conductivity across the field lines. When considering ISM, it is usually a valid assumption that the electrons are totally inhibited from moving across field lines (Braginskii 1965, McCourt et al. 2010). Under this assumption, the interface bounding the hot and cold materials will be significantly modified by the presence of tangled magnetic field, creating small structures at the field variation length scale. One typical example of such problems being the wind blown bubbles (WBB) which are observed to have hot bubble with observed temperature lower than expected (Zhekov et al. 2010). Many believe that heating through the hot bubble - cold shell interface via thermal conduction may have induced the cooling of the hot bubble (Zhekov et al. 1998, Zhekov et al. 2001). Meanwhile, the presence of the temperature gradient and global field will continuously cause materials of the cold side to evaporate, causing interface instabilities and mass mixing (Stone 2009), which would further modify the magnetic field topology. Another example is the unexpected slow cooling of the central galaxy core in the galaxy clusters, for which many suggest is a result of thermal conduction (Rosner et al. 1989, Balbus et al. 2008, Mikellides 2010). In the situation of intracluster medium (ICM), the tangled magnetic field often renders a hight anistropic thermal conductivity that may significantly change the temperature and density profile (Narayan et al. 2001, Mikellides et al. 2010). The key questions here are: (1) does the interface evolve into an instability driven by the anisotropic thermal conduction or a steady state stabilized by the anisotropic thermal conduction? (2) how fast is the thermal exchange between the hot and cold sides comparing to the isotropic thermal conduction case? In this paper, we visit the various situations with different magnetic field configurations imposed on a planar hot cold interface and study the effect of the tangled magnetic field on the evolution of the interface. Using ASTROBEAR code with anisotropic thermal conduction, we run simulations with different initial setup. In section 2, we review the

basic equations of MHD with anisotropic thermal conduction. Sections 3 and 4 provide detailed description of the simualtion setup, section 5 and 6 present the simulation results and analysis. In section 7, we apply the simulation results to astrophysical problems at different scales: the WBB cooling problem and the cooling flow problem in cores of galaxy clusters. The appendix offers detailed information on the testing of ASTROBEAR code.

2 MHD Equations with Anisotropic Heat Conduction

The MHD equations with anisotropic heat conduction are:

$$\frac{\partial \rho}{\partial t} + \nabla \cdot (\rho \mathbf{v}) = 0, \tag{1}$$

$$\frac{\partial (\rho \mathbf{v})}{\partial t} + \nabla \cdot [\rho \mathbf{v}\mathbf{v} + (p + \frac{B^2}{8\pi})\mathbf{I} - \frac{\mathbf{B}\mathbf{B}}{4\pi}] = 0, \tag{2}$$

$$\frac{\partial \mathbf{B}}{\partial t} + \nabla \times (\mathbf{v} \times \mathbf{B}) = 0, \tag{3}$$

$$\frac{\partial E}{\partial t} + \nabla \cdot [\mathbf{v}(E + p + \frac{B^2}{8\pi}) - \frac{\mathbf{B}(\mathbf{B} \cdot \mathbf{v})}{8\pi}] + \nabla \cdot Q = 0, \tag{4}$$

where E denotes the total energy:

$$E = \epsilon + p\frac{\mathbf{v} \cdot \mathbf{v}}{2} + \frac{\mathbf{B} \cdot \mathbf{B}}{8\pi} \tag{5}$$

and the internal energy:

$$\epsilon = \frac{p}{\gamma - 1} \tag{6}$$

with $\gamma = 5/3$. In our simulation, it is assumed that the heat flux is confined to be parallel to the magnetic field lines. This assumption is valid when the electron gyroradius is much smaller compared to the scale of the problem, i.e. the magnetic field strength has a threshold to let the anisotropicity to be effective. Under this assumption, the anisotropic heat flux can be written as:

$$Q = -\kappa_{\parallel} (\nabla T)_{\parallel} \tag{7}$$

where $\kappa_{\|}$ is the classical Spitzer heat conductivity. We assume the heat conductivity to be a constant throughout the simulation and will be writing it simply as κ.

The ASTROBEAR code uses operator splitting method to treat the MHD equations with heat conduction. The ideal MHD equations are solved with the MUSCL primitive method with TVD preserving Runge-Kutta temporal interpolation, the result is then sent to the implicit linear solver utilizing High Performance Preconditioners (HYPRE) to solve the anisotropic heat conduction equation. The linear solver requires temporal sub-cycling technique to maintain its accuracy. The time step taken by the linear solver can be written as:

$$t_{diff} = \frac{\rho l^2}{\kappa} \tag{8}$$

where l is the minimum scale length of the temperature variation: $l = min(T/|\nabla T|)$. The code runs in parallel with fixed grid domain.

3 Problem Description and Analytical Model

The problem involves a hot region representing hot material and a cold region representing cold material which are separated by a thin planar interface. The two regions are in pressure equilibrium. There is a magnetic field in the environment. We will study how the magnetic field configuration alters the heat transfer rate between the hot and cold regions.

Let us first consider two simple but illustrative cases: (1) a uniform magnetic field aligned with the normal direction of the interface; (2) a uniform magnetic field perpendicular to the normal direction of the interface. In case (1), because of the angle between the magnetic field and the temperature gradient is zero everywhere, the anisotropic heat conduction acts exactly the same as isotropic heat conduction. Thermal energy would transfer from the hot side to the cold side at a rate that only depends on the temperature distribution. In case (2) however, the angle between the magnetic field and the temperature gradient is always 90°, the thermal diffusion term in the energy equation is always zero. Thus the interface would stay unchanged. From the above two cases, we can see that if we define a

heat transfer rate η that is normalized by the transfer rate in the isotropic conduction case, namely:

$$\eta = \frac{q}{q_i} \tag{9}$$

then the average angle θ between the temperature gradient and the uniform magnetic field plays an important role in determining η. At $\theta = 0$, $\eta = 1$. At $\theta = \pi/2$, $\eta = 0$.

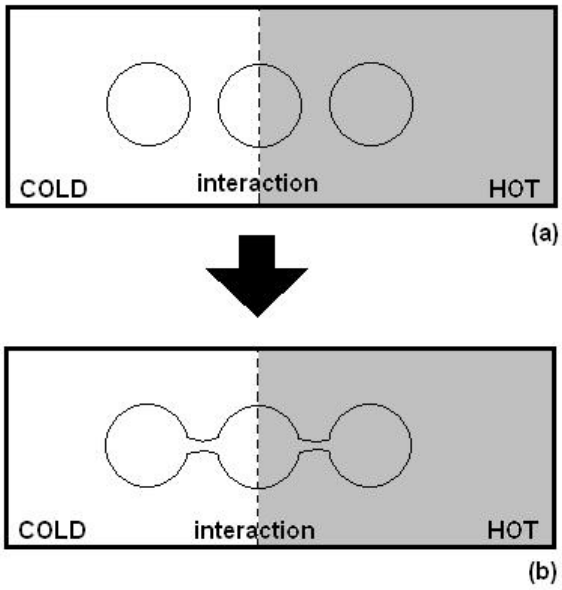

Figure 1: The initial and steady state field configuration. (a): the initial field forms complete circles that only allows heat transfer within the interaction region. (b): the steady state field reconnects itself so that it allows heat transfer between regions deeply into the hot and cold areas. We call the interaction region in (b) the "field membrane" because it allows the heat transfer between the hot and cold areas but the transfer is slower than the isotropic case since the heat flux is confined on the field lines.

The field configuration we consider next can be described as: there is a strongly tangled local field B_0 whose average on the normal of the interface is zero. There is also a global magnetic field B_d which is aligned

with the normal of the interface. There are three cases one can think of: (1) $B_d \gg B_0$, (2) B_d is comparable with B_0, (3) $B_d \ll B_0$. In the first case when the global field is strong, the magnetic field around the interface merely deviates from the normal direction. Thus one can imagine that this case would resemble case (1) in the uniform field situation and η should be close to 1. In the third case when the global field is weak, one would expect that there will be local energy redistribution, but the global energy transfer should be slow. Thus there will be an expansion on the interface, but the global temperature structure should remain unchanged and η should be close to zero.

In the second case however, one can only guess that η should be some value between zero and one. Another twist to the situation is the strucuture of the magnetic field. Consider the weak global field case. If the field is frozen into their positions, then one would imagine the region filled with the tangled field can have energy redistribution depending on the field topology, and then stay there since the field cannot move with the fluid elements. But if the field is frozen into the fluid elements, which is an assumption in ideal magneto-hydrodynamics calculation, one would expect that the field lines would redistribute themselves to keep up with the motion of the fluid elements. The question here is then: will this motion of field lines help the energy channeling or hamper it? If the feedback is positive, one would expect an acceleration of the energy transfer in the weak global field case, resulting in the destruction of the local field "wall", making the heat flux be able to penetrate through. Otherwise one would expect the global behavior of the interface to be the same as the case when the magnetic field is frozen into position, the local field "wall" would stay for a much longer period of time.

We define the tangled field region surrounding the interface as the "interaction region". Fig.1.(a) shows the initial and steady state field configuration in such a tangled field interface situation. From the figure we can see that initially the field forms a field wall since the field configuration does not allow the energy transfer between the two ends of the interaction region. But the steady state sees an expansion of the interaction region and magnetic reconnection which allows the field to penetrate through the entire region so that the field wall is destructed. In this paper, we will call

the destructed field wall as the "field membrane", which describes a stable region with tangled field distribution that allows a certain amount of heat to penetrate through in terms of anisotropic heat conduction, as in Fig.1.(b). We define the membrane's ability to block heat transfer as the "blocking rate", denoted by R_B. In the simple straight field situation we proposed before, $R_B = 0$ for the pure vertical field case, $R_B = 1$ for the pure horizontal field case. One way to define R_B is by defining it as the ratio between the mean B_y strength against the mean total field strength. Because of heat penetration, the thermal energy across the field membrane will see a certain jump which is determined by R_B. In the following study, we will check whether our assumption of the formation of field membrane is valid or not in the numerical simulation and quantitatively discuss its effect on the energy transfer.

4 Simulation Setup

To study the hot - cold interface energy transfer in circumstances such as the WBB, we construct the initial condition by setting up a hot - cold interface at pressure equilibrium. We will express the simulation parameters in computational units. Later we will see that our simulation can be used to describe certain real astrophysical situations once correct scaling parameters are chosen. The temperature follows the distribution:

$$T(x) = T_0(1 - x^2)^{1/2.5} \tag{10}$$

in the region of $0 < x < 1 - 10^{-5}$ with $T_0 = 100$ in computational units. The temperature distribution is plotted in pseudo color in Fig.2.(a). The region $0.4 < x < 0.5$ is the interaction region we defined in the previous section since it contains the sharp temperature gradient that would trigger the energy transfer process. At the two sides, the temperature is set to be constant and continuous from the ends of the interaction region. During the simulation, we are only interested in the region where the heat transfer can have a noticeable impact during the simulation run time. In other words, we will focus ourselves on the region surrounding the hot - cold interface, not regions deeply into the hot material. The horizontal length of the simulation domain is 0.1 in computational units. The thermal pressure is set to be in equilibrium:

$$P(x) = P_0 \tag{11}$$

with $P_0 = 100$ in computational units. The density distribution is set up by the perfect gas law, namely:

$$\rho(x) = \frac{P(x)}{T(x)} \tag{12}$$

For the Spitzer diffusion constant, we use the approximation of $\kappa = \kappa_c T_{mid}^{2.5}$, where κ_c is the classical conductivity, and T_{mid} is taken to be the middle value of temperature across the interface, which is about $0.6\,T_0$.

In our study, we choose the field configuration:

$$B_x = B_d + B_0 \sin(n\,\pi\,y/\lambda), \tag{13}$$

$$B_y = B_0 \sin(n\,\pi\,x/\lambda) \tag{14}$$

where n and λ are the mode number and wavelength of the tangled field respectively, $B_0 = 10^{-3}$ in computational units, and B_d can take various values but it is in general 1 order of magnitude smaller comparing to B_0. This field configuration creates a locally tangled field surrouding the interface. We can use ratio

$$R = B_d/B_0 \tag{15}$$

to describe the straightness of the magnetic field. $R = 0$ case indicates totally confined field lines, in which the field lines form sets of complete circles. $R = \infty$ case indicates straight field with all the field lines go from the hight temperature region to the low temperature region without any twist. One can imagine that with $0 < R < 1$, the field lines will be twisted and form sets of circles, but some of the circles are "incomplete" so that some of the field lines still go from the hot region into the cold region which become channels for energy transfer. In our simulation, we will consider cases with $R = 0.0,\ 0.2,\ 0.4,\ 0.6,\ 1,\ 2,\ 4,\ \infty$. Fig.2.(a), Fig.4.(a) and Fig.5.(a) show the magnetic field configuration for initial R values of 0.0, 0.4, 1.0.

We use fixed boundary condition on the x direction: the pressure, density and temperature at the two ends are fixed to their initial values so as the magnetic field. By this boundary condition, the two ends on the x axis can be seen as the regions deeply into the hot and cold regions, whose thermal dynamic variables stay constant. On the y axis, we use the periodic boundary condition.

There are five parameters involved in the simulation:

1. Magnetic β. β has little effect on diffuson since the field lines only determine the direction of the diffusion, but an extremely large β (weak field, or equivalently, the sound speed is much greater than the $Alf\acute{v}en$ speed) may affect the anisotropicity of the system. By contrast, an extremely small β may result in pressure imbalance in the initial condition. In our simulations, β falls in the range that it does not cause a strong pressure imbalance (the magnetic pressure is 10^{-8} in magnitude comparing to the thermal pressure), and also does not affect the anisotropicity (effective gyroradius is about 10^{-5} of the scale of the problem considered).

2. Tangle vs straight measure: $R = B_d/B_0$. If R is large, the local tangled field can mostly be ignored, we would get high energy transfer efficiency, and vice versa.

3. Ratio of the diffusion time scale and the hydrodynamic time scale: $r = t_{diff}/t_{hy}$. By simple physics consideration, we can have:

$$r = \frac{\rho\, C_s\, l}{\kappa} \tag{16}$$

where l is the characteristic scale length of temperature: $l = min(\frac{T}{|\nabla T|})$, C_s is the sound speed, κ is the linear diffusion constant. The initial kick is driven by the diffusion, the later evolution of the system depends on the value of r. If r is much smaller than 1, diffusion would dominate the initial phase and the pressure equilibrium may be broken by the fast energy transfer, if r is large, then the pressure equilibrium is well maintained throughout the entire process and the energy transfer may be viewed as a slow relaxation process. In the cases when the two time scales are comparable, both effects are present. In our simulation, $r \approx 0.3$ initially, so that the diffusion would trigger the heat transfer and pressure imbalance fastly at first. Then the hydrodynamics process would catch up and become faster than the diffusion process as a result of the decreasing of the temperature gradient and the fast expansion of the interface.

4. Ratio between the temperature scale length and the wavelength of the tangled field: $h = 2\,\pi\, l/\lambda = k\, l$ where l follows the same definition as

that in the previous paragraph. $h = 0$ marks the situation of no tangled field, which means there is nothing inhibitting the energy transfer. As h gets larger, the field becomes more confined, the energy is harder to transfer in the tangled field region, but a large h value may also result in a large chance of magnetic reconnection. The number of modes may also affect the result. We currently only look at the single mode case in which the spectrum is a delta function.

5. Mean global energy transfer rate: $\eta = 1/t_{bal}$, where t_{bal} can be defined as the time needed for the hot region and cold region to reach a certain degree of temperature equilibrium.

Next let us develop a simple mathematical expression for the heat transfer rate. Consider a slab with a sharp temperature interface aligned with the y direction and an average temperature gradient aligned on the x direction. There is an interaction region surrounding the temperature interface with tangled magnetic field in it. Define the global temperature gradient as $|\nabla T|_g = (T_{hot} - T_{cold})/(T_0\, L)$, where the subindices "hot" and "cold" denote the characteristic temperatures of the hot and cold regions, T_0 is a normalization factor which makes $|\nabla T|_g$ having dimension of $1/\text{length}$, L is the width of the interaction region. Then the energy transfer efficiency depends on how much the x component of the field B_x can penetrate through the interaction region. In other words, the averaged heat transfer rate from the hot region to the cold region should be:

$$\overline{q} = D\, \frac{|\nabla T|_g \int B_x\, dx\, dy}{\int |B|\, dx\, dy} \tag{17}$$

where D is a constant that depends on neither the magnetic field nor the temperature distribution, $|B|$ is the local field strength. Using Eqs.(12), (13) and (14), we find the approximated relation

$$\overline{q} \approx D\, \frac{|\nabla T|_g\, R}{\sqrt{1+R^2}} \tag{18}$$

Meanwhile, in the isotropic heat conduction case, the heat transfer rate purely depends on the temperature gradient:

$$\overline{q}_i = D\, |\nabla T|_g \tag{19}$$

Deviding Eq.(17) by Eq.(18), we get the heat transfer efficiency:

$$\eta = \frac{R}{\sqrt{1+R^2}} \tag{20}$$

Thus if the initial temperature profiles are identical for different field configurations, i.e. if $|\nabla T|_g$ are the same for the cases we are looking at, we can calculate the energy tranfer rate from situations with various field configuration and normalize them by the heat transfer rate of the isotropic heat conduction case to obtain the heat transfer efficiency. Later we will plot the heat transfer efficiency (η) against the field configuration (R) in our simulation results to verify relation Eq.(19).

If magnetic reconnection happens during the transfer process then channels can be opened up and the energy exchange process can be accelerated, we would expect the actual curve of η vs R to be higher than the value Eq.(19) predicts at regions where R is low. Meanwhile, at regions of high R, the analytical prediction and the real physical outcome should both approach the horizontal line $\eta = 1$, which denotes perfect efficiency. We can also write Eq.(19) in its general form:

$$\eta = \frac{\int \mathbf{B} \cdot \mathbf{G}\, dx\, dy}{\int |B|\, dx\, dy} \tag{21}$$

where **G** denotes the averaged global temperature gradient.

5 Simulation Result

We choose field set up with values $R = 0.0, 0.2, 0.4, 0.6, 1.0, 2.0, 4.0$ to run the simulations. The simulation run time is taken to be 1.2 which corresponds to 0.6 million years in real units. The initial cuts of temperature and magnetic field lines for $R = 0.0, 0.4, 1.0$ are shown in Fig.2.(a), Fig.4.(a) and Fig.5.(a) respectively. Fig.3.(a) shows the initial cut of the density distribution in the $R = 0.0$ run. We also run simulations with purely horizontal magnetic field lines which is equivalent to the $R = \infty$ case and purely vertical field lines. The rest frames in Fig.2 to Fig.5 are from the later stages of the evolution, and the final frames always display the steady state of the runs.

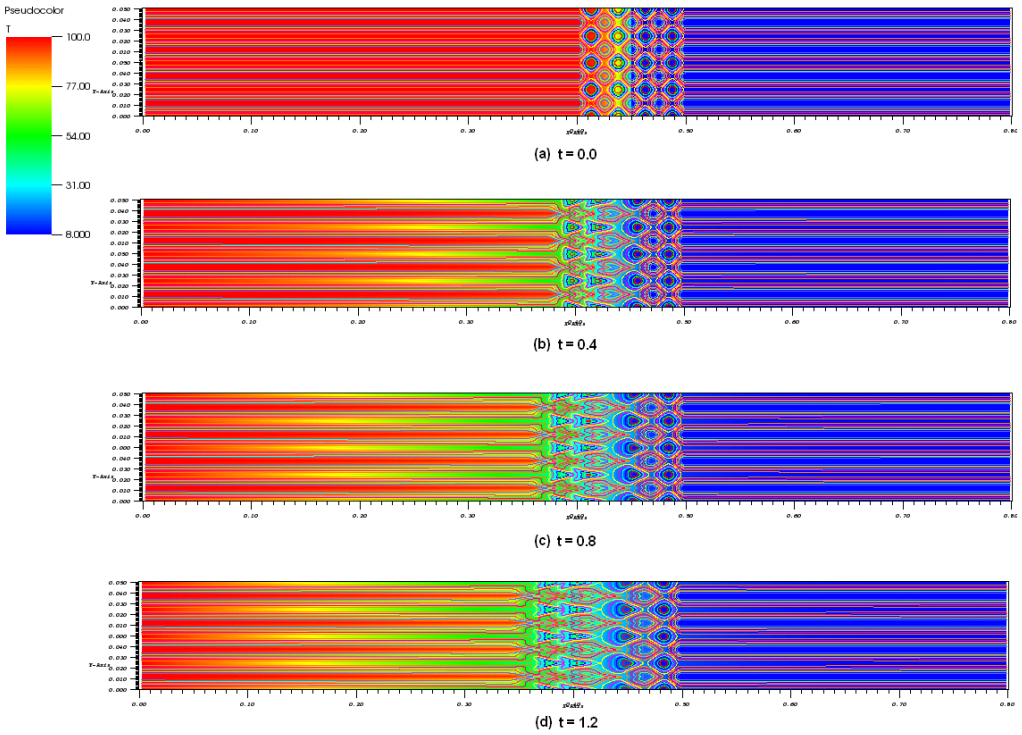

Figure 2: Evolution of temperature distribution with $R = 0.0$. The cuts are at (a): $t = 0.0$, the initial state, (b): $t = 0.4$, (c): $t = 0.8$, (d): $t = 1.2$, the steady state.

In Fig.6, we plot the mean cut temperature T_c against the x position for selected evolution time. T_c is obtained by averaging the temperature on the y direction, because the question we are interested in is how the heat transfer would perform along the x axis. Since initially the anisotropic heat conduction is faster than the hydrodynamic process, the energy distribution around the hot - cold interface will see a fast change until about $t = 0.4$. This energy transfer is mostly confined to the interaction region for the low R runs, because in these cases there are little to no field lines that can penetrate through the entire interaction region.

During this initial heat exchange phase, the thermal energy quickly redistribute itself in the interaction region as well as the density. As we can see from Fig.2.(b), islands at $x = 0.48$ are formed by materials bounded by the magnetic field lines, since they cannnot exchange heat with the envi-

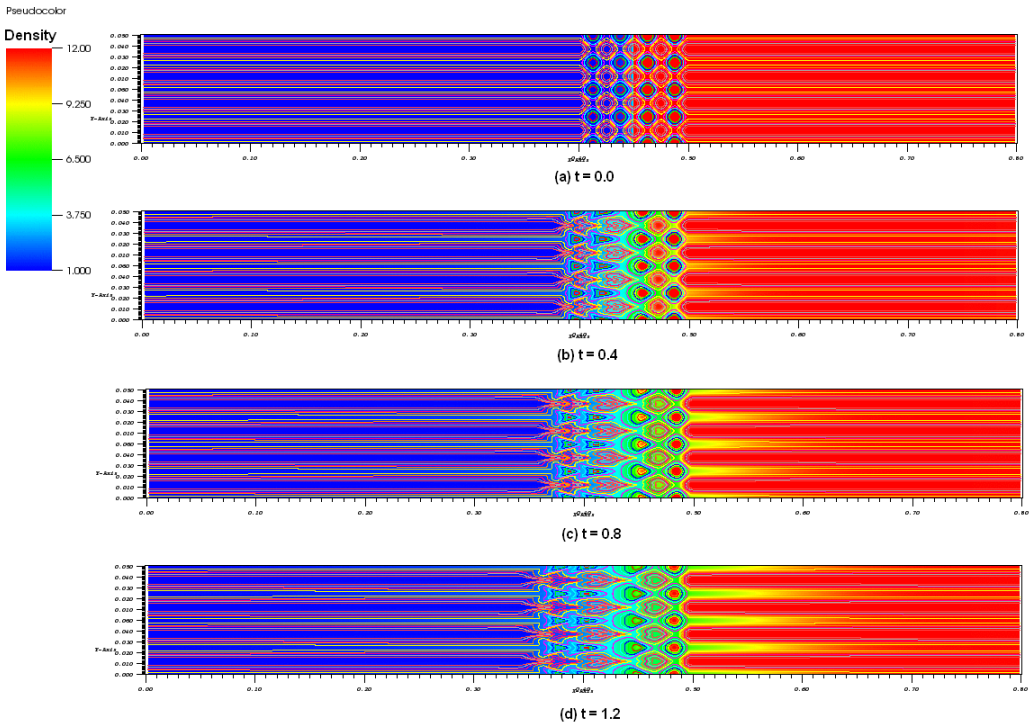

Figure 3: Evolution of density distribution with $R = 0.0$. The cuts are at (a): $t = 0.0$, the initial state, (b): $t = 0.4$, (c): $t = 0.8$, (d): $t = 1.2$, the steady state.

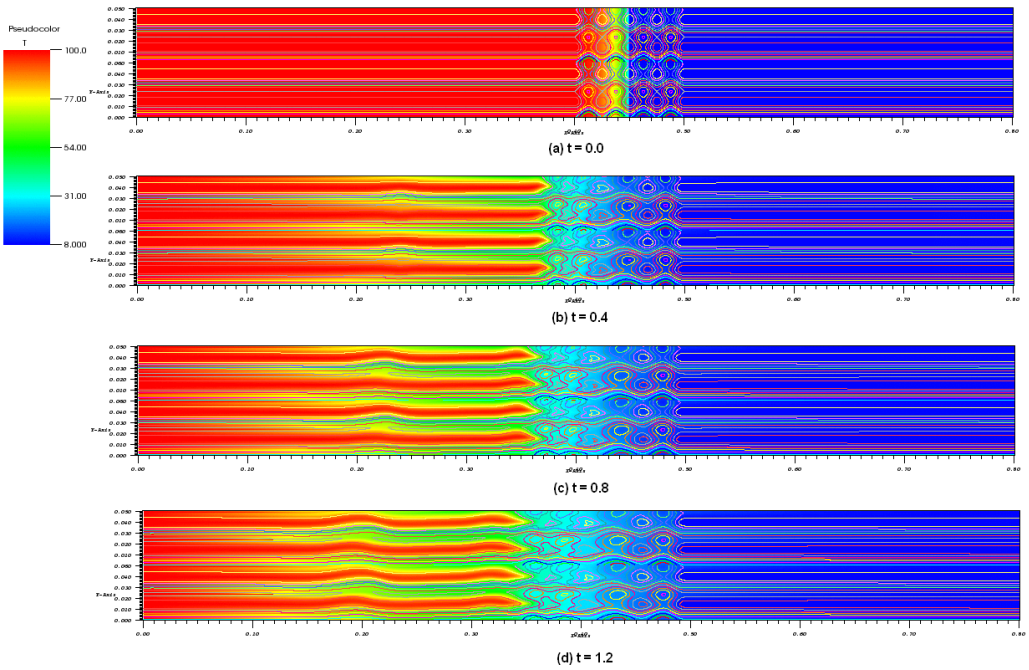

Figure 4: Evolution of temperature distribution with $R = 0.4$. The cuts are at (a): $t = 0.0$, the initial state, (b): $t = 0.4$, (c): $t = 0.8$, (d): $t = 1.2$, the steady state.

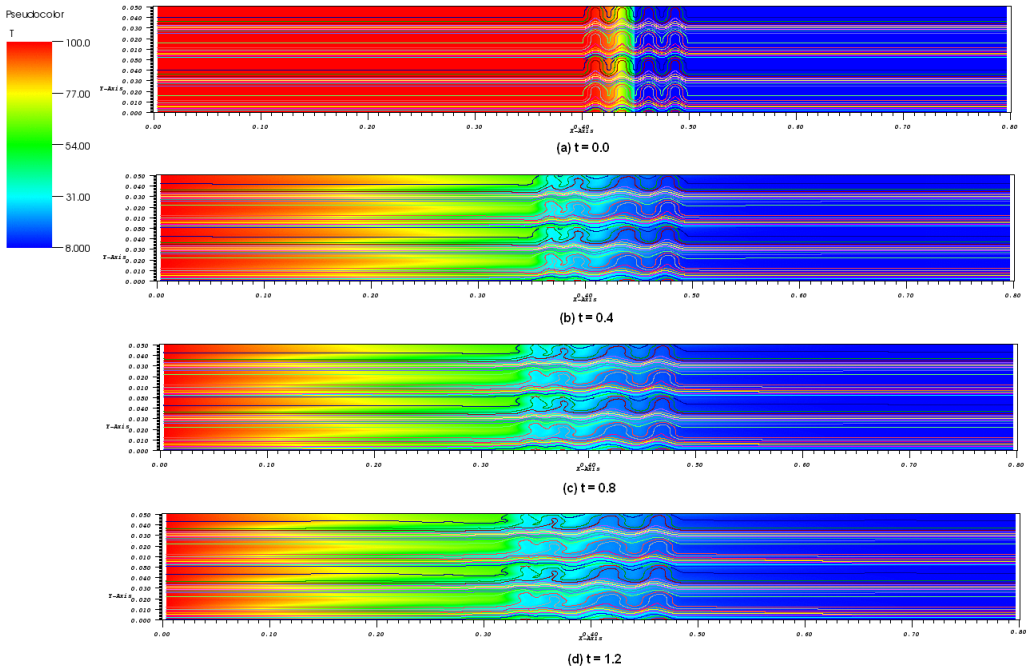

Figure 5: Evolution of temperature distribution with $R = 1.0$. The cuts are at (a): $t = 0.0$, the initial state, (b): $t = 0.4$, (c): $t = 0.8$, (d): $t = 1.2$, the steady state.

ronment.

The mass flow from the cold material pushes the interface, being heated up and forming an evaporation which is subject to interface instability because of the materials being accelerated to super-Alfven speed at the interface. This instability does not grow further but rather suppressed because the field lines are tangled rather than straight. There are also holes formed in between the spikes at around $x = 0.4$ because the thermal energy is inhibitted from flowing out of them. The magnetic field lines, which forms complete sets of circles in the $R = 0.0$ case, begin to distort. We can see that the field lines are distorted heavier in the low density part of the interaction region rather than in the high density part, because of the different speed they gain during the density redistribution. At time $t = 0.8$, we observe that the field lines surrounding the holes at $x = 0.4$ reconnect, making the thermal energy of the outter part of the holes begins to exchange.

Field lines that run from the high temperature region on the left side to the low temperature region deeply into the interaction region begin to emerge, causing the energy exchange to be possible between the hot side and the cold side. This phenomenon is more apparent in Fig.2.(d), which marks the final state of the thermal energy exchange. We also see that there are little difference between Fig.2.(c) and Fig.2.(d), because at the later stage of the process, the magnetic field configuration is approaching the steady state by which we mentioned as "field membrane" earlier in this paper. It is impossible for the temperature gradient to drive the material to move further at the steady state since the field membrane allows a certain degree of temperature jump to happen across it. This effect is also apparent by comparing Fig.6.(c) with Fig.6.(d), in which we observe that the mean cut temperature distribution changes little for all the different R values investigated. The mean cut temperature T_c sees a sharp jump in the region of $x = 0.35 \sim 0.5$, but is relatively smooth on the two sides. Because except for the interaction region which later becomes the field membrane and induces a temperature jump, the two sides of the domain are mainly governed by the heat conduction under horizontal magnetic field, which is identical to the situation of isotropic heat conduction.

For the cases of $R = 0.4$, there are field lines that penetrate the entire interaction region from the start. By observing the evolution of the magnetic field lines at about $x = 0.38$, we find that there are still magnetic reconnection happenning, which causes the magnetic blobs to merge. The observed behavior resembles the process displayed by Fig.(1). When $R = 1.0$, we can hardly find temperature islands that are bounded by magnetic blobs. The topological evolution of the field lines is better decribed as being straightened.

6 Discussion

We first analyze the evolution of heat flux. We plot the average heat flux for different R values in Fig.7.(a). From Fig.7.(a), we can see that the average heat flux for $R = \infty$ remains zero, which means the structure of the field totally forbids any transfer of heat across the interface. For $R = 1$, heat flux decreases because the temperature gradient is getting smaller in the transfer process. For the other R values (especially those of $R < 1$),

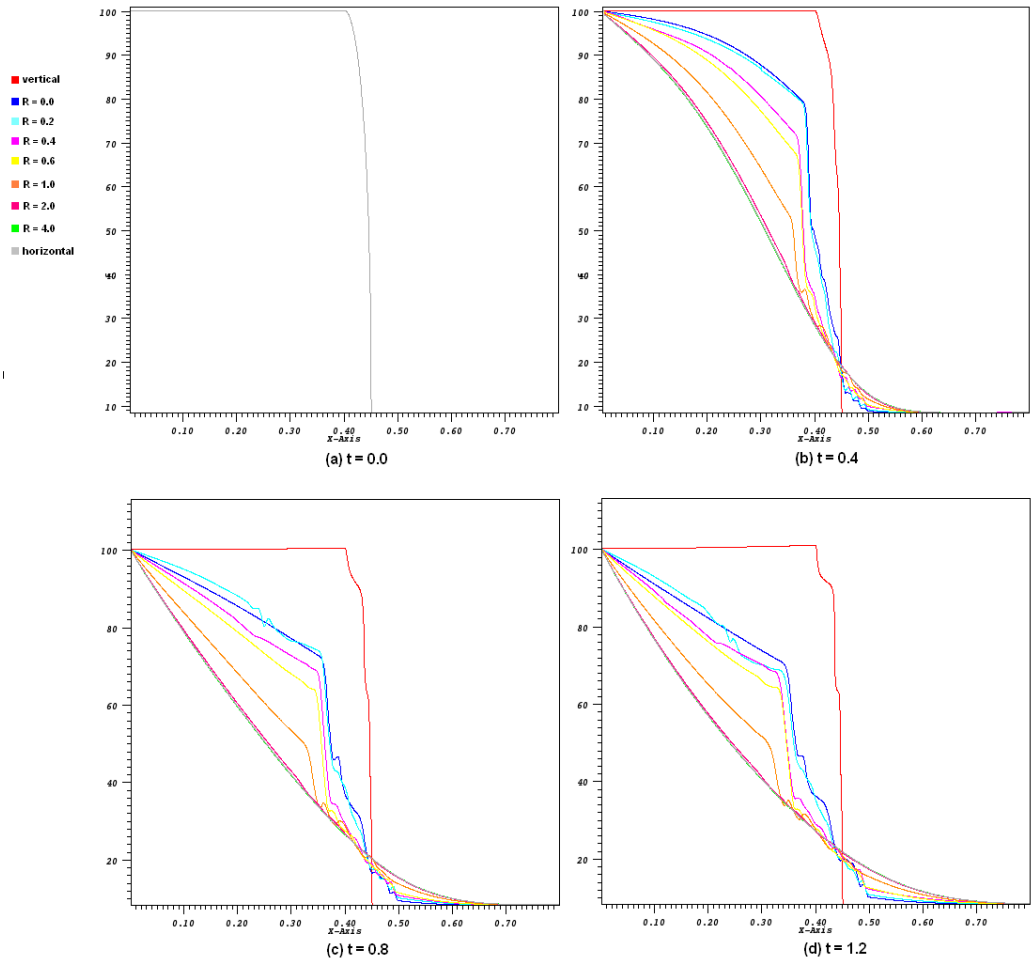

Figure 6: Evolution of mean cut temperature averaged on y direction with different R values labeled by different colors. The cuts are at (a): $t = 0.0$, the initial state, (b): $t = 0.4$, (c): $t = 0.8$, (d): $t = 1.2$, the steady state.

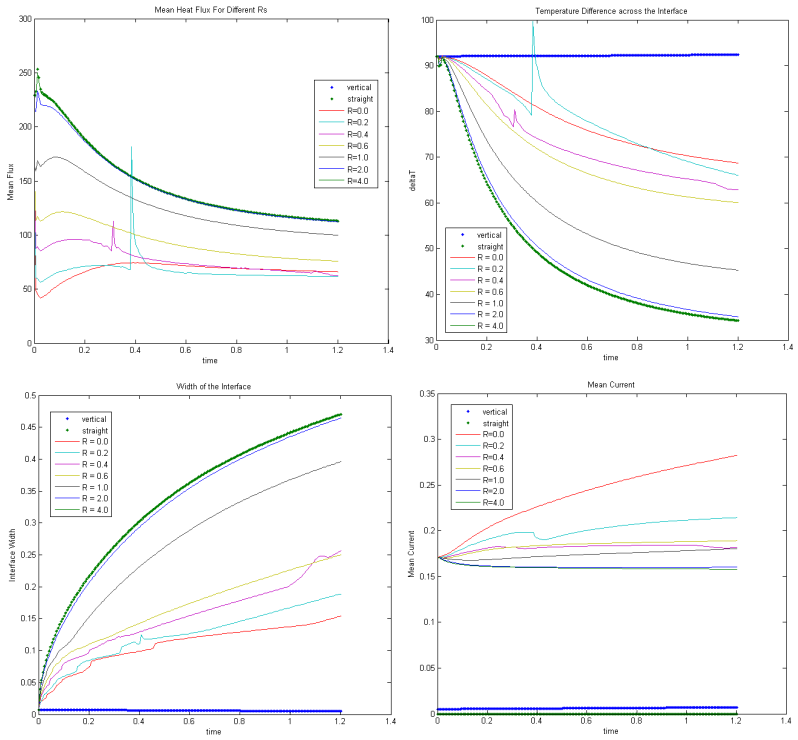

Figure 7: (a) top left: time evolution of mean heat flux at the interface, (b) top right: time evolution of average temperature difference between the hot and cold regions, (c) bottom left: time evolution of interface width, (d) bottom right: time evolution of the mean value of $|curl\mathbf{B}|$

one can see there is a phase of increasing heat flux. This may be caused by the magnetic reconnection openning up channels for heat to transfer from hot region to cold region. At the late stage of the evolution when there are enough channels opened up, the decreasing of temperature gradient becomes the dominating factor thus the overall effect is the average heat flux begins to decrease. We also see that the large R case resembles the $R = \infty$ case which is predicted by Eq.(20).

We next analyze the temperature equilibration across the interface. Fig.7.(b) shows the difference between the average temperature at the hot side and the cold side. One significant feature is that in all cases, the temperature

difference decrease to a steady value T_{end}. This resembles the percolation of a membrane which allows a density jump to happen when filtering two fluids. We also observe that the larger R is, the faster the energy transfer, and the smaller the temperature difference at the final steady state.

The third analysis considers how much the interface expands during the energy transfer. Fig.7.(c) shows the distance required for the temperature to drop from 60 to 10 at the interface. We can see except for the vertical field case when no heat transfer is allowed, the interface is expanding. We also see the large R case resembles the horizontal field case. The expansion for all the cases of nonzero R approach a steady value which is characteristic feature of the membrane effect.

Next, we analyze how the magnetic field configuration is changed by the energy equilibration process. Throughout our simulations, we use a local tangled field B_0 and a global straight field B_d. The local magnetic field is initially a set of complete circles surrounding the interaction region. Once the energy transfer begins to happen, the interaction region tends to expand as discussed previously. This expansion stretches the field lines on the x direction and results in the distortion of these circles, which eventually induces the magnetic reconnection which oppens up channels connecting the hot and cold regions. In out analysis, we use $J_B = |curl\mathbf{B}|$ as a characteristic value describing the degree of magnetic field tanglement. Fig.7.(d) shows the evolution of the mean value of the strength of $curl\mathbf{B}$ in the interaction region. We observe that in the vertical and straight field case, $|curl\mathbf{B}|$ remains constant, this is because the field configuration does not change during the process. $|curl\mathbf{B}|$ decrease to a fixed value for $R \geq 2$ cases, meaning the field in these cases is straightened by the stretching of the interaction region as seen in Fig.7.(c). For the $R \leq 1$ cases, $|curl\mathbf{B}|$ increase. This is due to the energy deposted into magnetic field in the interface instabilty with low R.

The distortion of the local field can be clearly demonstrated via studying the energy evolution. In Fig.8.(a), we plot the evolution of mean magnetic energy stored in the vertical field, namely $\bar{B}_y^2/2$, comparing to that stored in the mean horizontal field $\bar{B}_x^2/2$. Notice that here we only count in the tangled field part. From Fig.8.(a), we observe that the B_y energy decrease

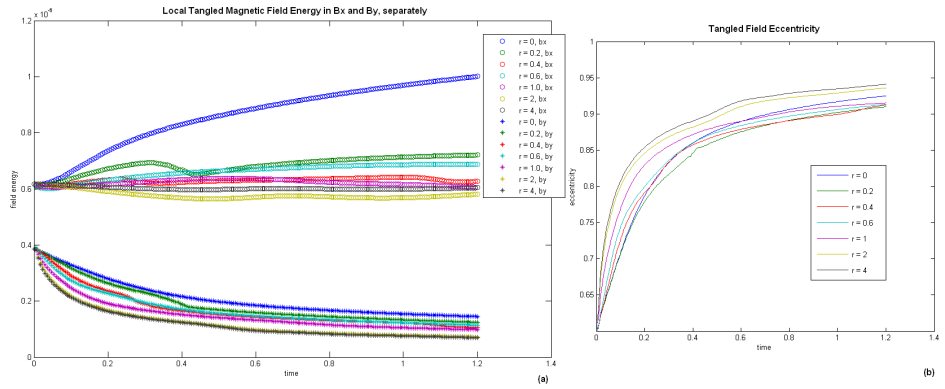

Figure 8: (a) Comparison on evolution of local field energy in terms of B_x and B_y. Circles corresponds to the $B_x^2/2$ curve, stars corresponds to the $B_y^2/2$ curve. The different colors denote various R values. (b) Eccentricity of the ellipses constructed by assigning the mean values of local $|B_x|$ and $|B_y|$ to the major and minor axes, respectively. The set of curves show different evolution patterns for different R values.

while the B_x energy either increase or stay stable for all cases. It can thus be viewed as a conversion of field energy from vertical pointing to horizontal pointing. However, reader needs to pay attention to the fact that this conversion may not conserve the total magnetic energy of the local tangled field, because of the existence of the induced interface instability and magnetic reconnection. By comparison, in the $R = 1$ case, the thermal energy and local magnetic energy would both decrease and add to the kinetic energy of the material surrounding the interface, because of the fast diffusion caused by the strong global field. The distortion of the local field circles can also be demonstrated if we regard them evolving into ellipses with major axis aligned with the x axis. The ellipse can be constructed by assigning the major axis to the mean value of $|B_x|$ and the minor axis to the mean value of $|B_y|$. In Fig.8.(b), we plot the evolution of the eccentricity of these ellipses. We see from the figure that large R cases tends to have greater eccentricity at the steady state. This is due to the fast expansion of the interface induced by the strong global field.

We next study the portion of B_y energy in the total magnetic energy by counting in the global field. Fig.9.(a) shows how the ratio of B_y energy

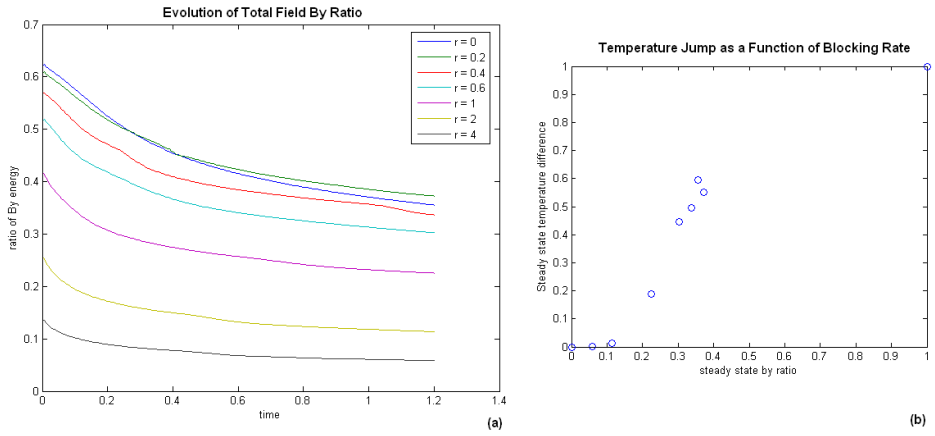

Figure 9: (a) The ratio of magnetic energy stored in terms of $B_y^2/2$ against the total magnetic energy. The set of curves show different evolution patterns for various R values. (b) The steady state blocking rate versus temperature jump. The blocking rate is obtained by calculating the proportion of mnagnetic energy stored in terms of B_y agains the total magnetic energy. The point $(0, 0)$ corresponds to the horizontal field situation, when there is neither temperature jump nor any blocking mechanism; while the point $(1, 1)$ corresponds to the vertical field situation, when the temperature jump is kept at the initial state value.

evolves with time. The decsending curve demonstrate that the ability for blocking the heat transfer is reduced by the mixing. We notice that the B_y energy ratio of the steady state negatively correlates with the initial R, which reminds us that it may be used as a characteristic parameter to describe the ability of blocking heat transfer at steady state. In Section 3, we proposed that the interaction region would evolve into a stable field membrane that allows a certain amount of heat flux to penetrate through and introduced a parameter R_B to describe the blocking rate of it. Let us use the definition of R_B proposed in Section 3: R_B is the ratio of the mean B_y strength against the mean total field strength. Thus we have:

$$R_B = \frac{\bar{B}_y}{|\bar{\mathbf{B}}|} \tag{22}$$

we notice that R_B is just the square root of the energy ratio we discussed in the previous paragraph. At the end of the simulation, R_B is relatively stable which denotes a steady state as discussed before. Fig.9.(b) plots the

steady state blocking rate against the relative temperature jump observed at the interface for the final state. Notice that the temperature jump is normalized by the initial temperature contrast across the interface. Therefore point $(0, 0)$ on the figure corresponds to the horizontal field situation when there is no temperature jump and no field structure that would block the heat flux. Point $(1, 1)$ denotes the vertical field situation when both the temperature jump and the field configuration stay at its initial state. Fig.9.(b) shows an ascending feature that agrees with our physics intuition that the greater the ratio of B_y energy in the total magnetic energy, the less transparent the field membrane would be. It should be mentioned that although both R_B and Eq.(20) describe the efficiency of the heat transfer through a modified interface, the definition of R_B does not contradict Eq.(20). The reason is that latter is an approximate equation and should be used as a rule of thumb to determine the energy transfer efficiency since it only depends on the relative strength of the local tangled field and the global field. By contrast, Eq.(22) depends on detailed field configuration and orientation. After addressing the evolution of the local tangled field, we finally come to the heat transfer rate in our simulations. Next we will verify how well Eq.(20) can approximate the heat transfer efficiency in our simulations.

To compute the estimated heat transfer rate in the simulation, we find out the average value of the slope in Fig.10, and compare it to the analytic model in Section 4. Here the average slope is calculated only in the region of the first quarter of the entire evolution time span, because the late stage sees a significant change in the magnetic field configuration which renders the analytic model invalid, especially for those low R value cases. From Fig.10, we can see that the two agree quite well except for the situation when R is below 0.2. The simulation result does not converge to point (0,0) but ends at an interception on the y axis. This interception indicates that even if there are few to no channels for energy transfer initially, the magnetic reconnection can open up channels and allow the heat transfer to happen. Eq.(20) is valid for predicting the cooling rate of the hot material throughout the early phase of the heat equilibration process. It also offers us insights on the strength of the local field strength around the interface once we know the cooling rate and the global magnetic field strength.

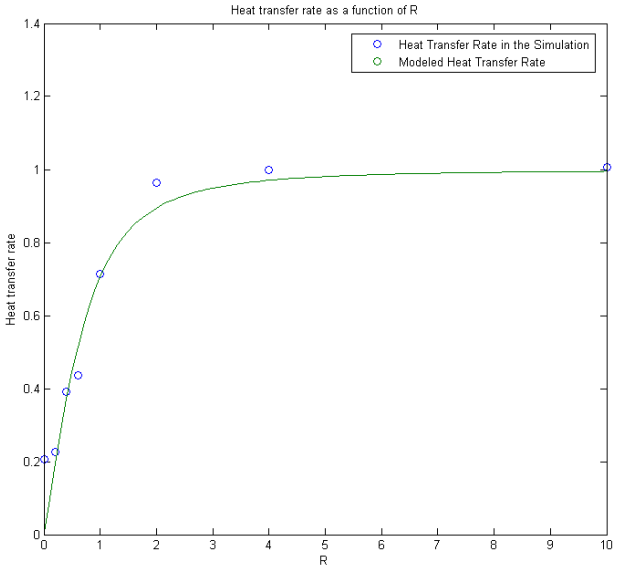

Figure 10: heat transfer rate observed in the simulation compared with the analytic model

In summary, the average total flux is in general a decreasing function for all R values, the curve also has an inital increasing phase which denotes the stage of strong magnetic reconnection. The average temperature difference decreases to a constant value T_{end} which is a function of initial R. Because of this feature, the magnetized interface can be viewed as an "energy membrane" that allows a certain energy jump to happen. The width of the interface expands to a fixed value during the simulation. The term that describes the structural change of the magnetic field is J_B. It decreases to a constant value for large R cases while increases to a constant value for small R values. The steady state blocking rate R_B is a function of R which can give us information about the structure of the steady state energy membrane. One can relate the steady state temperature jump T_{end} to the blocking rate R_B. We proved that Eq.(20) can be used to estimate the energy transfer rate in the case of complex field topology. It should be mentioned that Eq.(20) is a thumb of rule that can easily determine the heat transfer efficiency by considering the relative strength of the local

field and the global field.

7 Astrophysical Applications

The problem of magnetically modified hot - cold interface exist in many astrophysical contexts. One significant problem being the observed low temperature of the hot bubble in a Wind Blown Bubble (WBB) formed by a stellar wind. The WBB is predicted to have hot bubbles with a characteristic temperature greater than $2\,kev$, but the temperature observed from X ray emission detections is located at the $0.5\,kev$ to $1\,kev$ range (for details of observed NGC 6888, see Zhekov S.A. et al. 2010). This seemingly unnatural low temperature can be related to radiative cooling, or heat conduction. By scaling our computational data with the real physics data and putting into simulations, we find out two facts that are important in determining the actual temperature history of the WBB evolution: (1) the heat conduction existing in the WBB is strong enough to alter the evolution and impose an important influence on the temperature of the expanding hot bubble and the cold shell bounding it; (2) the magnetic field in the WBB, usually in the $1 \sim 10\,Gauss$ range, is usually strong enough to change the behavior of heat conduction. We can thus apply our analysis to the hot bubble - cold shell interface if we approximate the interface to be planar and stationary, which is accurate as the radius of WBB being much greater than the scale of the problem considered. We also assume that the global magnetic field is mostly radial. The computational parameters used in our simulations and the real physics parameters typical in a WBBis listed in the first two columns of Tab.1. We choose the domain length to be $0.1\,pc$, which is about 4 percent of the radius of the actual WBB. Tab.1 shows that by choosing the proper scaling, our simulation fits well with the data observed in a typical WBB. Therefore, the conclusions we draw by analysing the simulation results and the analytical expressions, especially Eq.(20), can be used in analysing real WBB evolution.

Variables	Computional Units	WBB	Galaxy
Number Density	1	$1\,cm^{-3}$	$10^{-2}\,cm^{-3}$
Temperature	100	$1\,kev$	$10\,kev$
Domain Length	0.1	$0.1\,pc$	$100\,pc$
Local Field Strength	10^{-3}	$10\,Gauss$	$1\,Gauss$
Global Field Strength	10^{-4}	$1\,Gauss$	$0.1\,Gauss$
Evolution Time	1.2	$0.6\,Myrs$	$13.3\,Myrs$
Heat Conductivity	10^{-2}	$2 \times 10^{-18}\,cm\,s\,g^{-1}\,K^{-2.5}$	$1 \times 10^{-17}\,cm\,s\,g^{-1}\,K$

Another important conclusion is that there exist a tangled field structure at the interface between the shell and the bubble, resulting in suppression of the thermal conduction and preventing the interface to expand further and turning into an isothermal distribution. One would also expect that dense spikes may stem from the cold shell side during the thermal energy transporting and evaporation phase because of the interface instabilty, leaving behind dense cold clumps bounded by magnetic field lines. The mass deposition onto the galaxy cores in clusters of galaxies, which is mainly induced by radiative cooling, would result in a cooling catastrophe if there is no certain heating mechanisms to heat up the cores of the central galaxies. However, the thermal conduction of the cool core clusters is unstable in that it may be either too weak to revert a cooling catastrphe or too strong so that it results in an isothermal temperature profile (Guo et al. 2008). The steady state of the local tangled field provide a possible solution to this problem since the temperature profile is controlled by the tangled field topology at the boundary of the central cluster. The tangled field provide a way of thermal exchange while preventing overheating. We scale the parameters in our simulation so that they match the cooling flow problem in ICM. One key difference is, in the ICM scenario, the cooling at the cool core cluster would reduce the cold side temperature profile to induce a further change at the boundary field membrane steady state. This may compose the topic of further numerical studies in this series.

8 Future Works

The future works of this study may include a multi-mode study, which investigates the impact of the spacial spectrum of the magnetic field dis-

tribution on the heat transfer efficiency and the topological evolution of the thermal dynamic variables. The interception on the y axis in Fig.13 indicates the R = 0 case heat transfer efficiency. It may be related to the mode number: the larger the mode number, the easier for the field to reconnect itself thus the higher the R = 0 tranfer rate. So considering the R = 0 case, there may be a dispersion relation that connects the efficiency to the mode number. When there are multiple modes or spectrum is continuous, it would be useful to predict how the efficiency would depend on the spectrum. We also know that the radiative cooling would be effective once the temperature is above $10^4\,k$. Since in our simulation the temperature has an order of magnitude of $10^7\,k$, the cooling would have a noticeable influence on the evolution. Another possible direction is to run the simulation of the hot cold interface with anisotropic heat conduction, radiative cooling, turbulence and gravity present.

Appendix: Code Test

We use the magneto-thermal instability (MTI) problem to test the accuracy of the ASTROBEAR code with anisotropic heat conduction. The problem involves setting up a 2D temperature profile with uniform gravity pointing on the y direction. The domain is square with length of 0.1 in compuational units. The temperature and density profiles are:

$$T = T_0\,(1 - y/y_0) \tag{23}$$

$$\rho = \rho_0\,(1 - y/y_0)^2 \tag{24}$$

with $y_0 = 3$. The pressure profile is set up so that the fluid can be balanced under uniform gravity with gravitational acceleration $g = 1$ in computational units. We also set $T_0 = 1$ and $\rho_0 = 1$ in computational units. There is a uniform magnetic field on the x direction with field strength $B_0 = 1.0 \times 10^{-3}$ in computational units. The anisotropic heat conductivity is set to be $\kappa = 1 \times 10^{-4}$ in computational units. We use the pressure equilibrium condition for the top and bottom boundaries, that is, the pressure in the ghost cells are set up so that its gradient can balance the gravitational force. On the x direction, we use the periodic boundary condition.

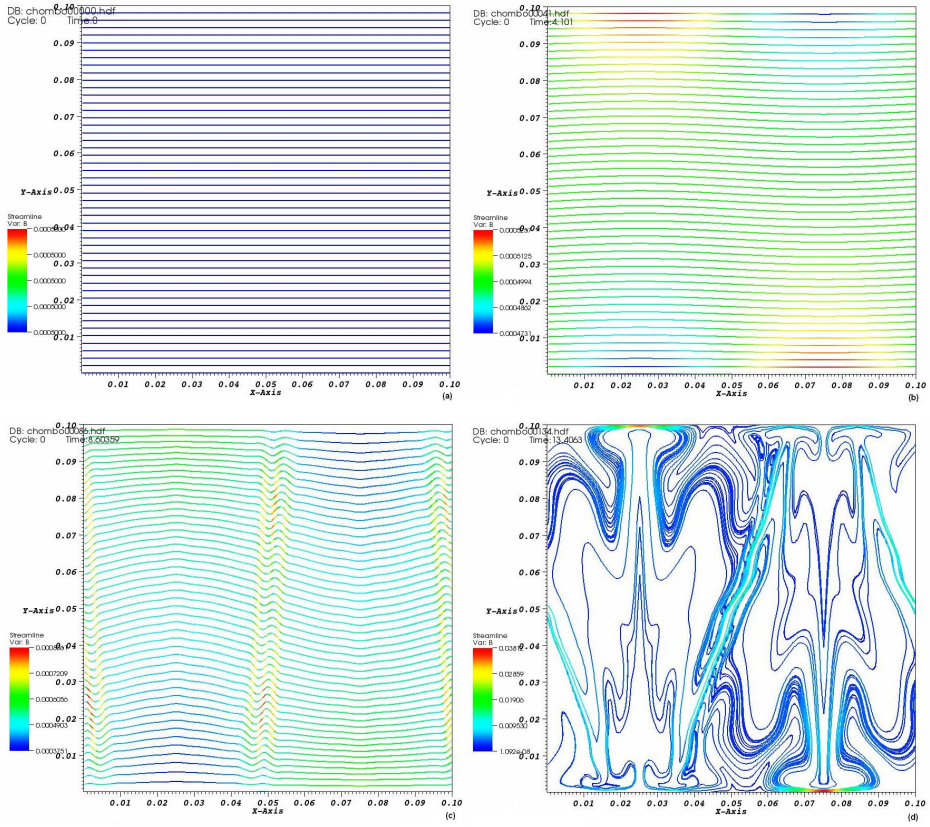

Figure 11: Field line evolution of magneto-thermal instability. (a): initial state. (b): $t = 75\tau_s$. (c)$t = 150\tau_s$. (d):$t = 250\tau_s$.

Initially, the domain is in pressure equilibrium. We then seed a small velocity perturbation:

$$v_{per} = v_0 \, \sin(n \, \pi \, x/\lambda) \tag{25}$$

with $v_0 = 1 \times 10^{-6}$ and $\lambda = 0.5$. This perturbation will cause the fluid elements to have a tiny oscillation on y axis as well as the field lines. Once the field lines are slightly bent, they open up channels for heat to transfer on the y direction thus allowing the heat on the lower half of the domain to flow to the upper half. It can be shown that this process has a positive feedback so that once the heat exchange happens, more channels will be openned up for heat conduction. Therefore this process forms an instabil-

ity whose growth rate can be verified according to the linear theory on the growth rate of weak field stratified atmosphere. We use τ_s to denote the sound crossing time for the initial state. Fig.11 shows the time evolution of the field lines at various stages in our MTI simulation.

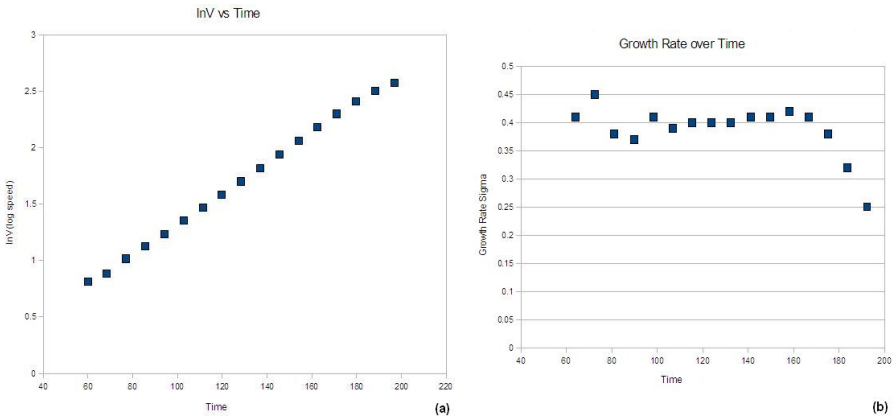

Figure 12: (a): $\ln v_y$ against evolution time in τ_s. (b): calculated growth rate against evolution time in computational units. Initially the growth rate is stable around the theoretical value 0.4 and then decreases sharply after $t = 200$, which indicates the evolution has entered the nonlinear regime.

We study the MTI growth rate by considering the acceleration of the fluid elements. The mean speed on the y direction for the fluid should follow the exponential growth:

$$v_y = v_{per} e^{\gamma t} \tag{26}$$

where v_{per} is the strength of the initial velocity perturbation applied, γ denotes the growth rate in the linear regime. We obtain the growth rate γ by plotting $\ln v_y$ against the evolution time and then measuring the local slope through a certain time span. The $\ln v_y$ vs t curve is plotted in Fig.12.(a), which shows a nice linear relation. We plot the growth rate against evolution time. It should be stable around the theoretical value 0.4 initially and then decrease sharply due to the nonlinear effect. Fig.12.(b). shows that the simulation meets our expectation fairly well.

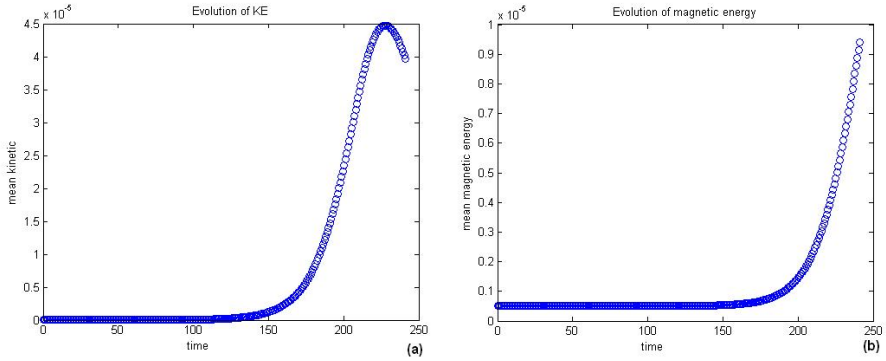

Figure 13: (a): evolution of mean kinetic energy. (b): evolution of mean magnetic energy.

Next we look at the energy evolution in the linear regime. The mean kinetic energy should first stay stable and then enter into an exponential growing phase until it hits a cap at around $t = 200$ which denotes the starting of the nonlinear phase. The evolution of magnetic energy should follow similar pattern as to the kinetic energy evolution, but lagged behind. In Fig.13, we plot the time evolution of the mean kinetic and magnetic energy evolutions. The results confirms the physical intuition quite well.

The dispersion relation of MTI can be expressed as a function of

$$\phi = (\gamma - 1)\,\frac{\kappa\, k^2}{N \rho_{mid}} \tag{27}$$

where $k = 2\pi/\lambda$, N is the $Brunt - V\ddot{a}s\ddot{a}l\ddot{a}$ frequency. Here we use the mid value of ρ. We can plot the MTI growth rate against ϕ to obtain the dispersion relation shown in Fig.14.(a).

Finally we study the impact of magnetic tension on the MTI growth rate. A strong initial field would provide a tension force that tends to stabilize the exponential growth. Thus intuitively the growth rate would be negatively correlated to the initial $Alf\acute{v}en$ speed. When the $Alf\acute{v}en$ speed approaches the value threshold value γ_{max}/k, we would expect a strong stabilizing tension to kill the instability growth. We use the stabilizing

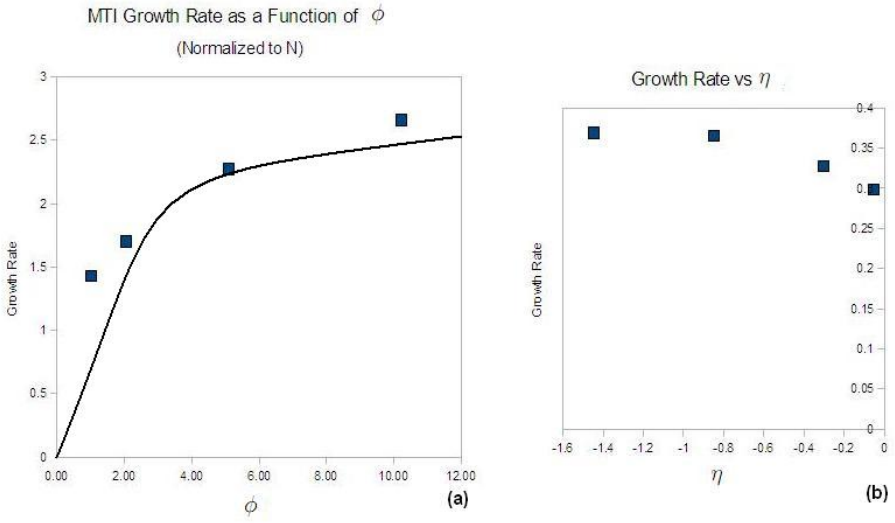

Figure 14: (a): the dispersion relation of MTI linear growth. (b): impact of field tension on the growth rate

parameter as a function of

$$\eta = \frac{k^2 v_A^2}{\gamma_{max}^2} \tag{28}$$

Here v_A is the initial maximum $Alf\acute{v}en$ speed, γ_{max} is the maximum possible growth rate which can be derived from the mid values of the initial temperature and pressure profiles. We plot γ against $\ln \eta$ in Fig.14.(b). We see that the field tension becomes increasingly effective as η approaching 1.